Computation of Sonar Performance Metrics Part 4

Marshall Bradley

This document illustrates how various types of uncertainty affect the forecasting of sonar performance in naval applications. The first type of uncertainty arises from the fact that we have incomplete knowledge regarding key target kinematic parameters such as range, bearing, depth, heading, speed, etc. In general key sonar performance metrics such as the sonar probability of detection P(D) are dependent upon each of these kinematic parameters. A second type of uncertainty is caused by the actual oceanographic environment in which the sonar operates. At a conceptual level, a sonar makes a mark on a gram or display when the voltage in a detector circuit exceeds a threshold. The probabilities with which these marks occur are determined by the statistics of the noise and signal that the sonar actually experiences. The statistical distribution of the signal and noise fields at the sonar receiver are strongly influenced by a nondeterministic component of ocean sound transmission. Numerous examples are presented.

Background

This document was originally written in 2010 when the author was a scholar in residence at Southeastern Louisiana University. It is presented here in a slightly updated format. In some instances the Mathematica code for computing the figures has been included. The original document contained an introduction and six sections. The section on example computation of sonar performance metrics is presented here. The author is currently the Chief Scientist at LogLinear Group, LLC.

marshall.bradley@gmail.com
September 2022

6.0 Example computations of sonar performance metrics

6.1 Azimuthal independent ocean with spherical spreading propagation

In this section we will consider the case of an azimuthal independent ocean with a flat bottom. We will assume that sound propagation can be computed via simple spherical spreading. We will consider two target scenarios. In the first scenario, target probability density is uniform in range and bearing out to a distance of 10000 yd. In the second scenario, target probability density is uniform in range and bearing out to a distance of 20000 yd. Functionally, the probability density in either case is described by

$$P(r) = \frac{r}{\frac{1}{2} r_{\max}^2},$$

where $r_{\max}$ = 10 000 yd in scenario 1 and $r_{\max}$ = 20 000 yd in scenario 2. The probability density function $P(r)$ is often referred to as the prior target range probability density function or the prior range distribution.

We will consider an omnidirectional passive sonar employing a matched filter detector with integration time T = 1 sec and false alarm rate of p_{fa} = 10^(–6) that operates in an ambient noisefield with spectral noise level AN = 80 dB re 1 μPa $/ \sqrt{\text{Hz}}$. The target source level is assumed to be SL = 160 dB re 1 μPa. If r denotes distance from the target to the sonar receiver, then the signal to noise ratio on an intensity scale is

$$snr(r) = \frac{T\, 10^{\frac{SL}{10}} r_0^2}{10^{\frac{AN}{10}} r^2},$$

where r_0 is a reference distance of 1 yd. The probability of detecting a target at range r is

$$P(D \mid r) = \Phi\left(\sqrt{2\, snr(r)} - z_{pfa}\right),$$

where Φ(z) is the cumulative distribution function for a standard normal Gaussian probability distribution and z_{pfa} is the solution of the equation $p_{fa} = 1 - \Phi(z_{pfa})$. For p_{fa} = 10^(–6), z_{pfa} = 4.75342. A plot of $P(D \mid r)$ is shown in figure 6.1.

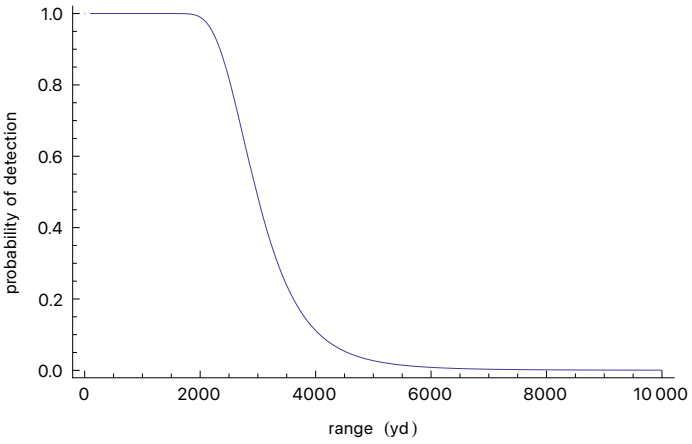

Figure 6.1. Probability of detection for an omni directional passive sonar in a 20 $\log_{10}(r)$ environment. Source level, ambient noise spectral level, system integration time and false alarm rate are respectively 160 dB, 80 dB, 1 sec and 10^(–6).

We will consider 3 measures of sensor performance. These are the sensor probability of detection $P(D)$, the sensor half-sweep width $W_{1/2}$ and the posterior range probability distribution $P(r \mid D)$. This last quantity is the answer to the question, "What is the probability of target range given a detection?". It can be computed using Bayes theorem. As discussed in section 2, these quantities are in an azimuthal invariant environment defined by the following equations:

$$P(D) = \int_0^{r_{max}} P(D \mid r)\, P(r)\, dr = \frac{1}{\frac{1}{2} r_{max}^2} \int_0^{r_{max}} P(D \mid r)\, r\, dr,$$

$$W_{1/2} = \int_0^{\infty} P(D \mid r)\, dr,$$

$$P(r \mid D) = \frac{P(D \mid r)\, P(r)}{\int_0^{\infty} P(D \mid r)\, P(r)\, dr} = \frac{P(D \mid r)\, r}{\int_0^{r_{max}} P(D \mid r)\, r\, dr}.$$

The sensor probability of detection $P(D)$ is strongly dependent upon the prior range distribution $P(r)$ as evidenced by the appearance of the r_{max} term in the denominator of the defining equation for $P(D)$. When r_{max} becomes large, the numerator in this expression approaches a finite value due to the rapid decay in $P(D \mid r)$ with range for large r. The numerator becomes infinite and $P(D)$ tends to zero regardless of the character of $P(D \mid r)$. By way of contrast, the sensor half-sweep width $W_{1/2}$ is totally independent of $P(r)$. The posterior range distribution $P(r \mid D)$ will effectively independent of $P(r)$ provided that r_{max} extends out into the region where sensor performance is poor.

Performance metrics associated with the posterior range distribution $P(r \mid D)$ are the expected detection range $E[r]$ defined as the mean of the posterior target range distribution:

$$\bar{r} = E[r] = \int_0^{\infty} r\, P(r \mid D)\, dr,$$

and the expected detection probability $\bar{p}_d$ defined as the expected value of the probability of detection $P(D \mid r)$

$$\bar{p}_d = E[P(D \mid r)] = \int_0^{\infty} P(D \mid r)\, P(r \mid D)\, dr.$$

A plot of the prior target range distribution $P(r)$ and the posterior target range distribution $P(r \mid D)$ are shown in figure 6.2 Figure 6.3 shows the posterior range distribution $P(r \mid D)$ for scenarios 1 and 2. The distributions are essentially identical. So long as r_{max} is greater than about 8000 yd, the posterior range probability density distribution will be insensitive to the choice of r_{max}.

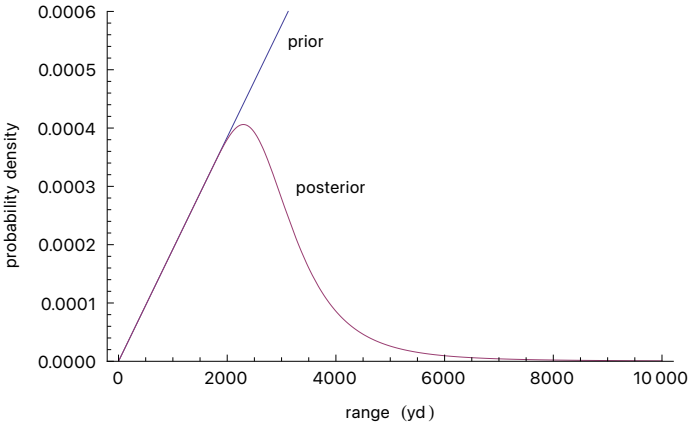

Figure 6.2. Posterior and prior target range distributions for scenario 1.

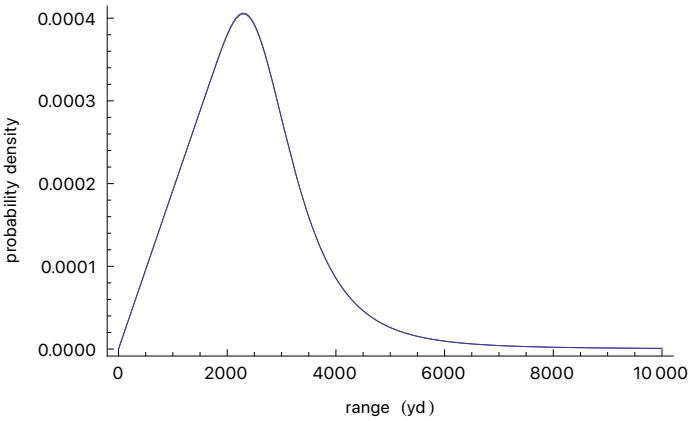

Figure 6.3. Posterior target range distributions for scenario 1 and 2. The distributions are nearly identical.

Table 6.1 summarizes values of $P(D)$, $W_{1/2}$, $\bar{r}$ and $\bar{p}_d$ for scenario 1: r_{max} = 10 000 yd and scenario 2: r_{max} = 20 000 yd. As can be seen from the table, the sensor probability of detection is very sensitive to the value of r_{max}. As r_{max} increases, the target probability density is spread over a wider area and $P(D)$ decreases. The performance metrics $W_{1/2}$, $\bar{r}$ and $\bar{p}_d$ are insensitive to the values of r_{max} except for specialized circumstances.

Metric	*Scenario 1*	*Scenario 2*
$P(D)$	0.104	0.0261
$W_{1/2}$	3129 yd	3130 yd
$\bar{r}$	2393 yd	2422 yd
$\bar{p}_d$	0.734	0.732

Table 6.1. Performance metrics for scenario 1 and 2.

In order to further examine the dependence of the performance metrics $P(D)$, $W_{1/2}$, $P(r \mid D)$, $\bar{r}$ and $\bar{p}_d$ on the prior target distribution, we will assume that the sensor probability of detection for a target at range r is the step function

$$P(D \mid r) = \begin{cases} p_0, & r_0 < r < r_1 \\ 0, & \text{otherwise} \end{cases}$$

where p_0 is a constant between 0 and 1, and let us again assume that the target prior range distribution is

$$P(r) = \frac{r}{\frac{1}{2} r_{max}^2},$$

where $r_{max} > r_1$. Then the performance metrics $P(D)$, $W_{1/2}$, $P(r \mid D)$, $\bar{r}$ and $\bar{p}_d$ can be computed in closed form. The results of these computations are shown in table 6.2. The sensor probability of detection is strongly dependent upon the choice of r_{max}. The other performance metrics are independent of r_{max} provided that $r_{max} > r_1$.

Performance Metric	*Value*	*Dependence on P(r)*

$P(D)$	$p_0 \, {r_1^2 - r_0^2} \Big/ r_{\max}^2$	strong
$W_{1/2}$	$p_0(r_1 - r_0)$	none
$P(r \mid D)$	$r \Big/ \left(\frac{1}{2}\left(r_1^2 - r_0^2\right)\right)$	none
$\overline{r}$	$\frac{2}{3}\left(r_1^3 - r_0^3\right) \Big/ \left(r_1^2 - r_0^2\right)$	none
$\overline{p}_d$	p_0	none

Table 6.2. Performance metrics for an analytic scenario.

6.2 Short and long range sonar comparison

We will consider the performance of two sonars. The first is a short range sonar, perhaps a sonobuoy, with detection capabilities out to 2000 yd. The second sonar is a longer range sonar with detection capabilities out to 8000 yd. We will consider two target distribution scenarios. In scenario 1 the target probability density $P(r)$ is uniformly distributed in range and azimuth out to the maximum effective range of the sonar (either 2000 yd or 8000 yd). Thus in the first scenario, the prior target range distribution is chosen to match the detection performance of the sonar. In the second scenario, the target probability density is uniformly distributed over a square-shaped region that is 1000 kyd by 1000 kyd and the sonar is assumed to be located at the mid point of the square.

We will assume that the sensor lateral range $P(D \mid r)$ is given by the analytic function

$$P(D \mid r) = \text{Exp}\left[-4 \frac{r^2}{r_0^2}\right],$$

where r_0 = 2000 yd for sonar 1 and r_0 = 8000 yd for sonar 2. A plot of this function is shown in figure 6.6. At short ranges, both sonars have probability of detection values near 1, but at longer ranges, sonar 2 is clearly superior. The posterior range distributions $P(r \mid D)$ for scenarios 1 and 2 and sonars 1 and 2 are shown in figure 6.7. Even though the prior range distributions $P(r)$ are very different as evidenced by figures 6.4 and 6.5, the posterior range distributions $P(r \mid D)$ are very similar.

The performance metrics $P(D)$, $W_{1/2}$, $P(r \mid D)$, $\overline{r}$ and $\overline{p}_d$ for the two scenarios are shown in table 6.3. For scenario 1 in which the target prior range distribution is matched to the sonar detection range, we see that sonar 1 and sonar 2 have the the same $P(D)$ value of 0.245 even though sonar 2 has 4 times the detection range of sonar 1. This highlights the fact that using $P(D)$ as a performance metric should only be done if the goal is present some type of location specific or relative measure of sonar performance. If the goal is compare the performance of different sonars, then different performance metrics should be used. As we saw in section 6.2, the probability of detection $P(D)$ is very sensitive to the target prior range distribution. The other performance metrics are not sensitive to the target prior range distribution.

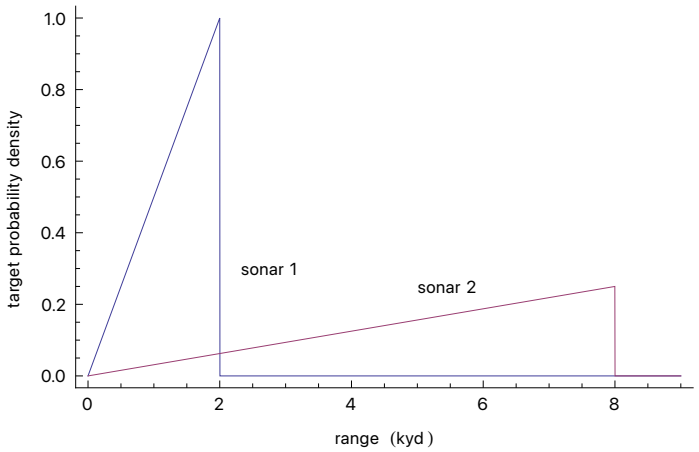

Figure 6.4. Prior target range distributions $P(r)$ for scenario 1.

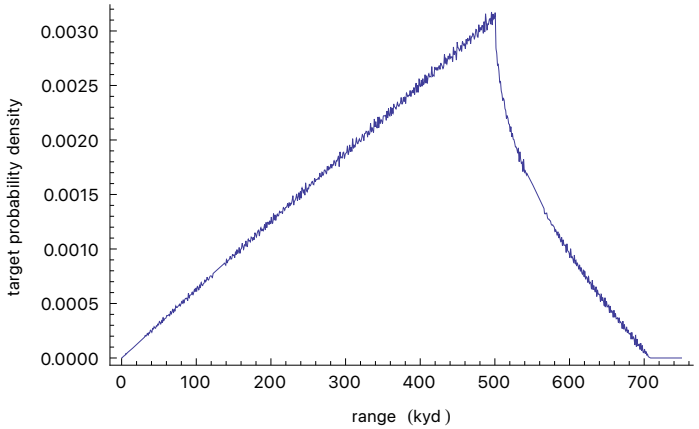

Figure 6.5. Prior target range distributions $P(r)$ for scenario 2.

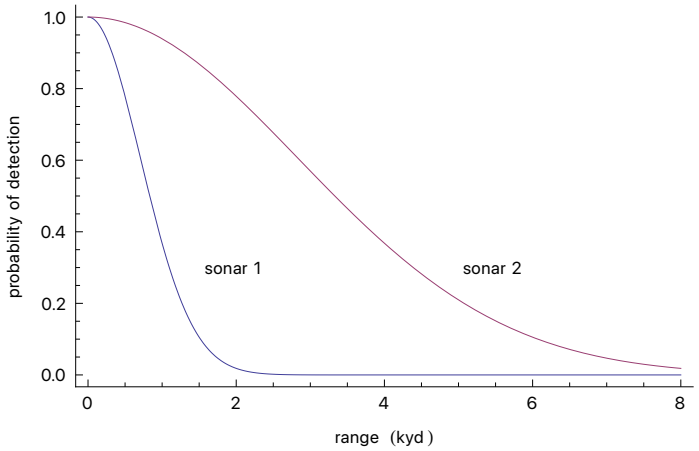

Figure 6.6. Sensor lateral range $P(D \mid r)$ for sonar 1 and sonar 2.

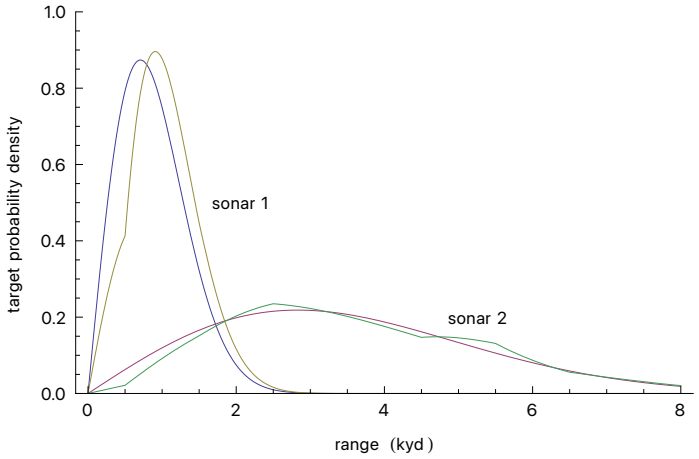

Figure 6.7. Posterior range distributions $P(r \mid D)$ for scenario 1 and scenario 2. Scenario 1 is represented by the smooth curve in blue. Sonar type 1 and 2 is indicated in the figure.

Performance Metric	*Scenario 1 Sonar 1*	*Scenario 1 Sonar 2*	*Scenario 2 Sonar 1*	*Scenario 2 Sonar 2*
$P(D)$	0.245	0.245	3.31×10^{-6}	4.92×10^{-5}
$W_{1/2}$	0.882 kyd	3.53 kyd	0.882 kyd	3.53 kyd
$\overline{r}$	0.861 kyd	3.44 kyd	1.04 kyd	3.69 kyd
$\overline{p}_d$	0.509	0.509	0.401	0.478

Table 6.3. Performance metrics for two prior target range distributions and two sonar types. In scenario 1 the target prior range distribution is matched to the characteristics of the sonar. In scenario 2 the target probability density is spread out over a very wide area.

6.3 Convergence zone sonar

In the examples we have considered so far, sonar performance as measured by the lateral range curve $P(D \mid r)$ has been assumed to monotonically decrease with range r. This is not always the case. In certain deep water ocean environments with favorable sound velocity variation with depth, sonars can achieve detections at ranges out to 50 kyd via convergence zone (CZ) propagation. In order to investigate this phenomena, we will assume that the sensor lateral range $P(D \mid r)$ can be mathematically represented by the functional form,

$$P(D \mid r) = \exp\left[-\left(\frac{r}{w_d}\right)^2\right] + 0.8 \exp\left[-\left(\frac{r - r_{cz}}{w_{cz}}\right)^2\right],$$

where w_d is the nominal direct path detection range, r_{cz} is the range to the center of the convergence zone and w_{cz} is the convergence zone width. Figure 6.8 shows a plot of this function with $r_d = 5$ kyd, $r_{cz} = 50$ kyd and $w_{cz} = 1.5$ kyd. The choice of the value 0.8 in the defining expression for $P(D \mid r)$ was made for illustrative purposes. The sonar achieves detection via direct path propagation out to about 10 kyd. Convergence detections occur in a narrow range band centered on a range of 50 kyd.

We will consider two target scenarios. In the first scenario, the target probability density $P(r)$ is assumed to be uniformly distributed in range and azimuth out to a range of 60 kyd. This range was

chosen to be just beyond the maximum detection range of the sonar. In the second scenario, the target probability density is uniformly distributed over a square-shaped region that is 1000 kyd by 1000 kyd and the sonar is assumed to be located at the mid point of the square. A plot of $P(r)$ for the second scenario is shown in figure 6.5.

As we have previously discussed, the posterior probability density $P(r \mid D)$ is the answer to the question what is the probability of range given detection. It is computed via the Bayesian formula

$$P(r \mid D) = \frac{P(D \mid r)\, P(r)}{\int_0^\infty P(D \mid r)\, P(r)\, dl\, r},$$

where $P(D \mid r)$ is the sensor lateral range curve and $P(r)$ is the prior target probability distribution. For the CZ sonar case, $P(r \mid D)$ for scenario 1 and scenario 2 is shown in figure 6.9. Even though the prior target probability densities are very different, the posterior distributions are similar. The performance metrics $P(D)$, $W_{1/2}$, $P(r \mid D)$, $\bar{r}$ and $\bar{p}_d$ for the two scenarios are shown in table 6.4. As we have previously seen in sections 6.1 and 6.2, the value of the sensor probability of detection,

$$P(D) = \int_0^\infty P(D \mid r)\, P(r)\, dl\, r,$$

again is strongly dependent on the choice of the prior distribution $P(r)$ but the other performance metrics are not. For the CZ sonar, the half seep width $W_{1/2}$ does not adequately reflected the extended detection range of the sonar.

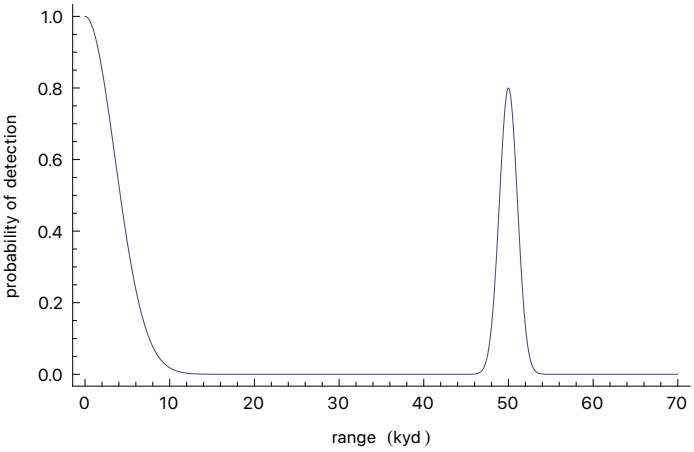

Figure 6.8. Sensor lateral range $P(D \mid r)$ for a convergence zone sonar.

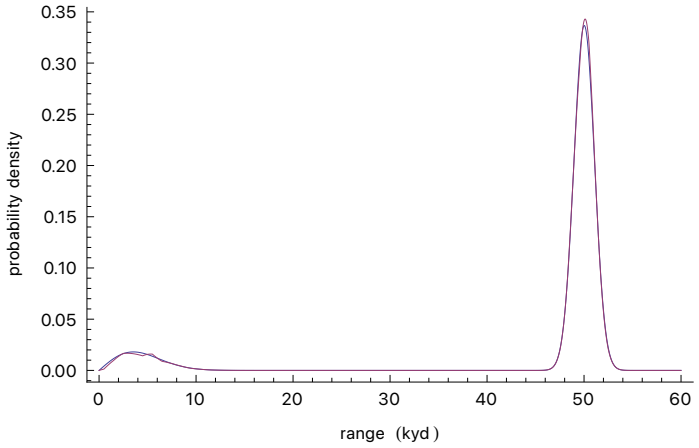

Figure 6.9. Convergence zone sonar posterior range distributions $P(r \mid D)$ for scenario 1 and scenario 2. Scenario 1 is represented by the smooth curve in blue. The posterior distributions are very similar.

Performance Metric	*Scenario 1*	*Scenario 2*
$P(D)$	6.60×10^{-2}	7.49×10^{-4}
$W_{1/2}$	6.56 kyd	6.56 kyd
$\overline{r}$	45.2 kyd	45.6 kyd
$\overline{p}_d$	0.559	0.559

Table 6.4. Performance metrics for a convergence zone sonar.

6.4 Performance surface for minehunting sonar in a region with spatial variation in bottom backscatter

In the examples we have considered so far, we have ignored the effects that spatial variation in the ocean environment has on system probability of detection $P(D)$ and other related performance metrics. We will now consider a scenario in which the spatial variation of the environment plays an important part. To this end, we consider the following scenario: A naval ship is searching a shallow-water ocean area that is 5000 yd by 4000 yd in size. The ship is trying to find a target (mine) that is lying on the bottom. The ships's high-frequency-active sonar is operated in a reverberation limited mode and makes detection via a direct propagation path. The search region is divided into two parts as shown in figure 6.10. Region 1 is an area of low bottom backscatter and region 2 is a region of high bottom backscatter. We anticipate that sonar performance will be much better in region 1 due to reduced reverberation masking levels.

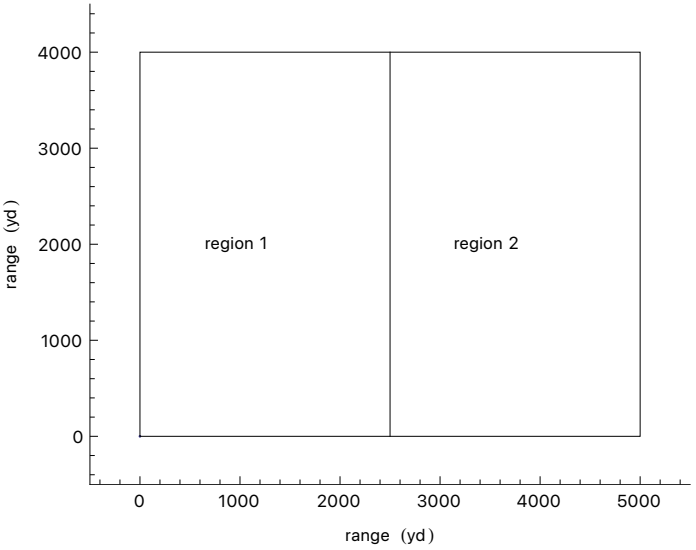

Figure 6.10. Plan view environmental geometry for the mine-hunting sonar example. Regions 1 and 2 are respectively areas of low and high bottom backscatter. Active sonar performance is better in region 1 relative to region 2 due to lower reverberation levels.

The signal to mask (*snr*) ratio which the sonar achieves against a target at slant range R when the sonar employs a short CW pulse of length t_p can be written in the form

$$snr(R) = \left(10^{\frac{SL}{10}}\, b_p(\phi)\, b_r(\phi)\, \frac{10^{\frac{-2\,\alpha\, R}{10}}}{R^4}\, 10^{\frac{TS}{10}} \right) \Bigg/ \left(10^{\frac{SL}{10}}\, b_p(\phi)\, b_r(\phi)\, \frac{10^{\frac{-2\,\alpha\, R}{10}}}{R^4}\, \sigma_{\text{back}}(\theta)\, R\, \Phi_{\text{hor}}\left(c\, t_p / 2\right) + \frac{1}{t_p}\, 10^{\frac{AN}{10}}\, DF \right).$$

The numerator in this expression is the target echo and the denominator is the mask. The two terms in the denominator are the bottom reverberation and noise power measured in the receiver bandwidth. In this expression SL is the projector source level, TS is the target strength, AN is the ambient noise spectral level, DF is the receive array directivity factor (not dB), Φ_{hor} is the receiver horizontal beam width and c is sound speed. We assume that soundspeed is constant. The projector and receiver beam patterns at launch angle ϕ are denoted by $b_p(\phi)$ and $b_r(\phi)$, and $\sigma_{\text{back}}(\theta)$ is the bottom backscatter function at grazing angle θ. If the target is lying on the bottom and the sonar projector is operated at sufficiently large levels with the sonar steered towards the target, then bottom reverberation is the dominant masking component and

$$snr(R) = \frac{10^{\frac{TS}{10}}}{\sigma_{\text{back}}(\theta)\, R\, \Phi_{\text{hor}}\left(c\, t_p / 2\right)}.$$

A computation of sonar signal to noise ratio (*snr*) has been performed using the sonar and environmental parameters shown in table 6.5 and the bottom backscatter models shown in figure 6.11. The results of this computation are shown in figure 6.12. As can be seen by examining the figure, sonar performance is manifestly better in region 1. Sonar signal to noise ratio for a bottom-lying target is shown in figure 6.13. Figure 6.13 is just a horizontal slice (or cut) through figure 6.12 at the depth of the bottom (500 ft).

We will assume that the minehunting sonar employs an envelope detector with characteristics illustrated in figure 6.14. The mapping from signal to noise ratio to probability of detection shown in figure 6.14 is used to produce the lateral range curves $P_1(D \mid r)$ and $P_2(D \mid r)$ for regions 1 and 2 as shown in figure 6.15. Probability of detection versus horizontal range r is clearly better in region 1 than in region 2. This results from the fact that region 1 has lower bottom backscatter and better sonar signal to noise ratio.

Parameter	*Value*	*Parameter*	*Value*
Source level	224 dB re 1 μPa	Pulse length	1 ms
Frequency	80 kHz	Receiver bandwidth	1000 Hz
Tilt	20 deg down	Receiver noise	51 dB re 1 μPa$/$Hz$^{1/2}$
Horizontal beamwidth	1.7 deg	Target strength	0 dB
Vertical beam width	20 deg	Water depth	500 ft
Source depth	100 ft	Wind speed	5 kt

Table 6.5. Sonar and environmental parameters.

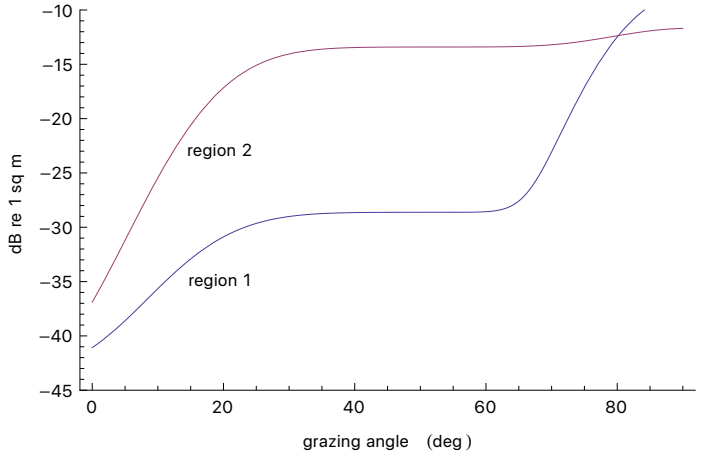

Figure 6.11. Bottom backscatter models for region 1 and region 2.

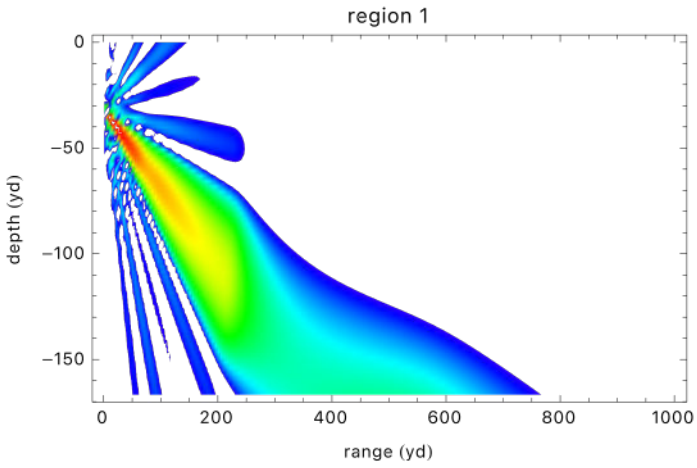

Figure 6.12-1. Color display of sonar signal to noise ratio (*snr*) in region 1 (low bottom backscatter) and region 2 (high bottom backscatter). Results are are presented on a 0-60 dB range with warm colors corresponding to high *snr* values.

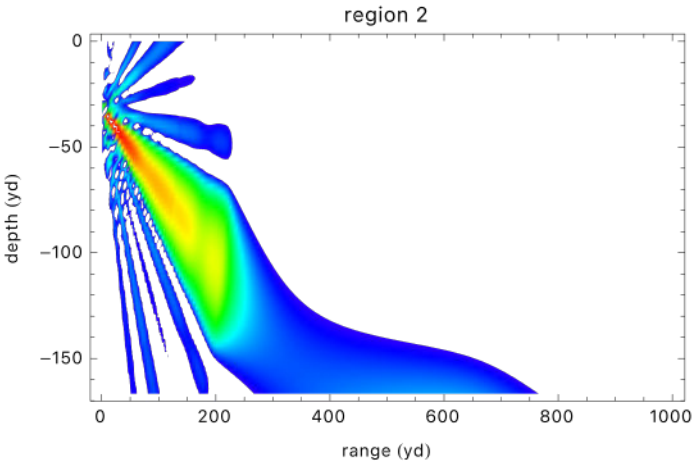

Figure 6.12-2. Color display of sonar signal to noise ratio (*snr*) in region 1 (low bottom backscatter) and region 2 (high bottom backscatter). Results are are presented on a 0-60 dB range with warm colors corresponding to high *snr* values.

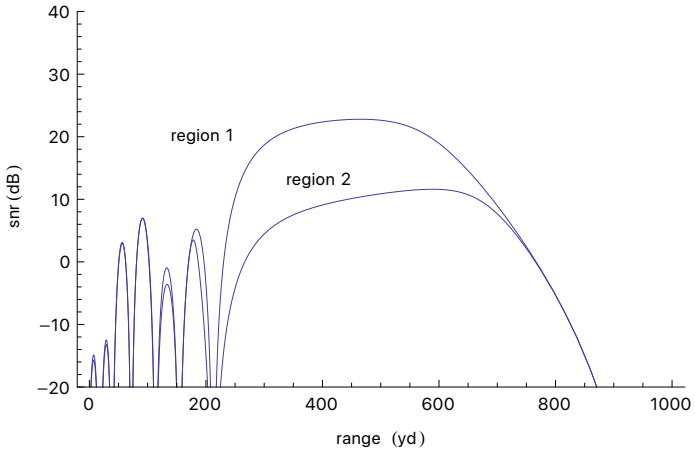

Figure 6.13. Sonar signal to noise ratio (*snr*) for bottom-lying target in region 1 (low bottom backscatter) and region 2 (high bottom backscatter).

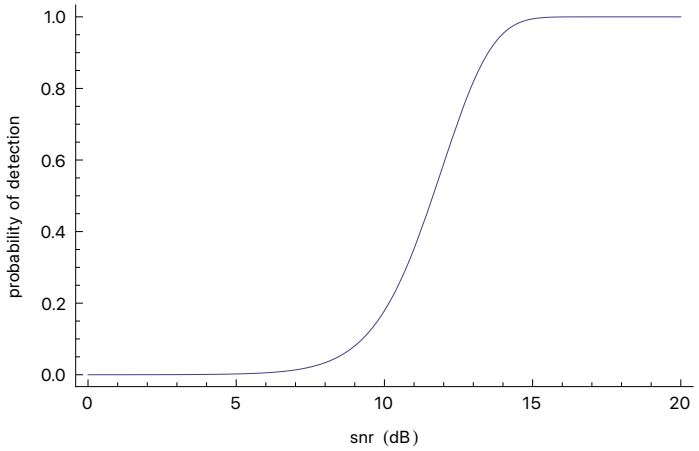

Figure 6.14. Conversion from sonar signal to noise ratio (*snr*) for to probability of detection for a sonar employing an envelope detector with a false alarm rate of 2.8 * 10 ^ (−7) .

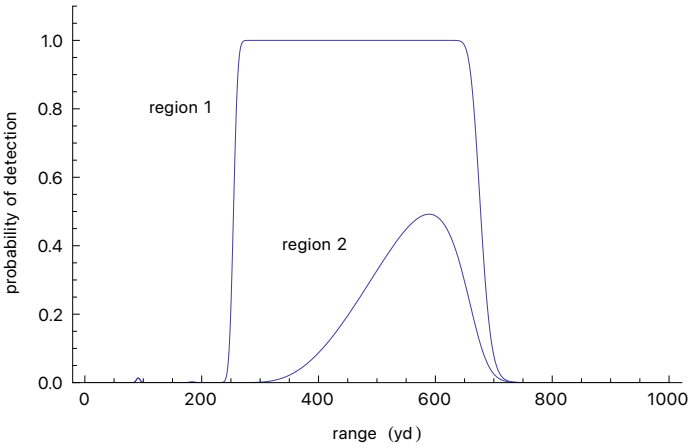

Figure 6.15. Sonar lateral range curves $P_1(D \mid r)$ and $P_2(D \mid r)$ in regions 1 and 2 for a bottom lying target. The false alarm rate is 2.8*10^(–7).

We now turn our attention to the computation of sonar probability of detection for a given receiver location (x_r, y_r) which we will denote by $P(D \mid x_r, y_r)$. A computation or plot of this quantity is sometimes referred to as a performance surface. Since sonar performance is sensitive to the location of the sonar and the target, we make this computation by marginalizing over the target location (x_t, y_t). In order to do this, we will assume that the target location is uniformly distributed over the region depicted in figure 6.10. This assumption implies that the the target probability density function is given by

$$P(x_t, y_t) = \frac{1}{x_{\max}\, y_{\max}},\ 0 < x < x_{\max},\ 0 < y < y_{\max}$$

0, otherwise.

where $x_{\max}$ = 5000 yd and $y_{\max}$ = 4000 yd. The performance surface $P(D \mid x_r, y_r)$ is then

$$P(D \mid x_r, y_r) = \int_0^{x_{\max}} \int_0^{y_{\max}} P(D \mid x_r, y_r, x_t, y_t)\, P(x_t, y_t)\, dx_t\, dy_t.$$

Due to the simple nature of $P(x_t, y_t)$, we can compute $P(D \mid x_r, y_r)$ via

$$P(D \mid x_r, y_r) = \frac{1}{x_{\max}\, y_{\max}} \int_0^{x_{\max}} \int_0^{y_{\max}} P(D \mid x_r, y_r, x_t, y_t)\, dx_t\, dy_t.$$

In this example, the spatial dependence of sonar performance enters our computations through the target location. If the target location is in region 1, then we compute $P(D \mid x_r, y_r, x_t, y_t)$ via $P_1(D \mid r)$. If the target location is in region to then we use $P_2(D \mid r)$ where $P_1(D \mid r)$ and $P_2(D \mid r)$ are defined in figure 6.15. The horizontal range r in either case is simply

$$r = \left[(x_r - x_t)^2 + (y_r - y_t)^2\right]^{1/2}.$$

A computation of the performance surface $P(D \mid x_r, y_r)$ over a discrete set of receiver grid locations (x_m, y_n) is shown in figure 6.16. There are several distinct areas in the figure. There is a flat, plateau shaped area corresponding to the center portion of region 1 in figure 6.10. In this area, sonar performance is relatively high because nearby targets are more likely to be located in a region of low bottom

backscatter. There is another flat, plateau shaped area corresponding to the center portion of region 2 in figure 6.10. In this second area sonar performance is not as good because nearby targets are more likely to be located in a region of high bottom backscatter . There is also a sloped transition area between regions 1 and 2. Additionally, near the boundaries of the region shown in figure 6.10, the performance surface values $P(D \mid x_r, y_r)$ decay due to geometrical edge effects. If the receiver is on or near the boundary, then range to a random target location is more likely to be larger than if the receiver location was well removed from the boundary. This edge effect biases $P(D \mid x_r, y_r)$ towards lower values whenever (x_r, y_r) is located near a boundary. It simply reflects the fact that $P(D \mid x_r, y_r)$ depends on the product of $P(D \mid x_r, y_r, x_t, y_t)$ and $P(x_t, y_t)$ through the range map defined by the previous equation.

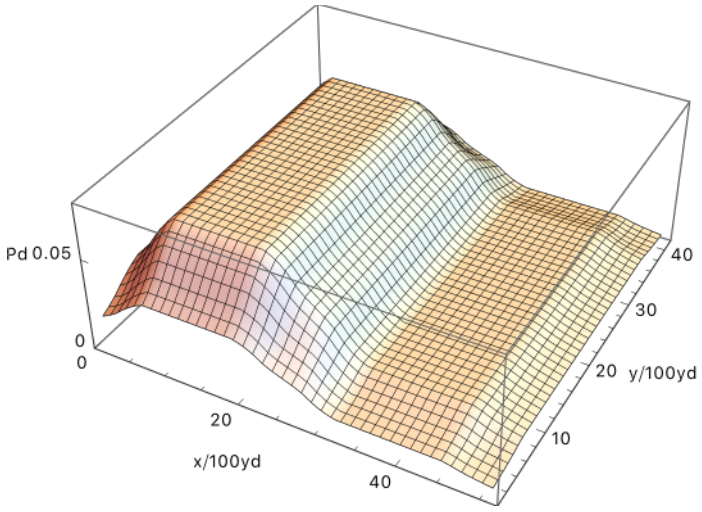

Figure 6.16. Computation of the performance surface $P(D \mid x_r, y_r)$ via marginalization over the target probability density $P(x_t, y_t)$.

The performance surface $P(D \mid x_r, y_r)$ can also be computed by a Monte Carlo simulation. As we shall see this is not a computationally efficient process. However, the monte Carlo approach does intuitively correspond to the idea of repeated, random engagements between a sonar and a target. This is the type of engagement that occurs in some naval campaign models. The first step in the MonteCarlo Simulation is to randomly generate a pair of receiver and target location $\{(x_r, y_r), (x_t, y_t)\}$ and to compute the range from receiver to the target. Next we compute a realization of probability of detection

$p_d = P_{1\,\text{or}\,2}(D \mid r)$,

where $P_{1\,\text{or}\,2}(D \mid r)$ means use the lateral range cure for region 1 if the target location (x_t, y_t) is in region 1. If the target location is in region 2, then the lateral range cure for region 2 is used to compute p_d. The third step is to respectively accumulated probability of detection and opportunity into separate arrays $\alpha(x_m, y_n)$ and $\beta(x_m, y_n)$ where (x_m, y_n) represent a two-dimensional discretization of receiver locations over the region $\{(0, x_{\max}), (0, y_{\max})\}$. If the array indices m and n are such that $x_m \le x_r < x_{m+1}$ and $y_n \le y_r < y_{n+1}$, then $\alpha(x_m, y_m)$ is incremented by p_d and $\beta(x_m, y_n)$ is incremented by 1. The arrays $\alpha(x_m, y_n)$ and $\beta(x_m, y_n)$ are initially set to zero before the Monte Carlo process is begun. A large number of realizations are required before meaningful estimates can be made. In the example under discussion

in this session, we used 1,000,000 realizations. Once the Monte Carlo looping process is finished, $P(D \mid x_m, y_n)$ is estimated via

$$P(D \mid x_m, y_n) = \frac{\alpha(x_m, y_n)}{\beta(x_m, y_n)},$$

which is simply the ratio of accumulated probability divided by accumulated opportunity. The results of the Monte Carlo simulation are shown in figure 6.17.

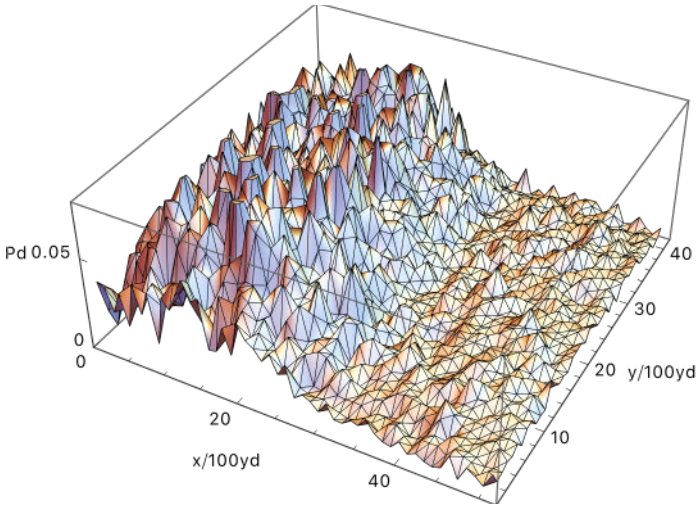

Figure 6.17. Computation of the performance surface $P(D \mid x_r, y_r)$ via Monte Carlo simulation with 1,000,000 realizations.

Cuts through figures 6.16 and 6.17 at the position y_r = 2000 yd are shown in figure 6.18. The smooth line corresponds to the cut through the performance surface computed via the marginalization process. The jagged lie is the cut through the Monte Carlo simulation. There is clearly agreement between the two approaches. However, even at 1,000,00 realizations, the Monte Carlo computation has only partially converged to the marginalization computation.

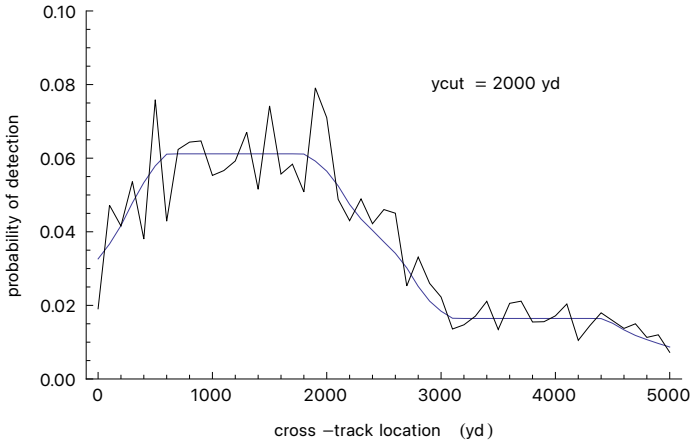

Figure 6.18. Computation the marginalization and Monte Carlo computations of the performance surface $P(D \mid x_r, y_r)$.

Referring to figure 6.18, the probabilities of detection in the plateau regions centered on x_r = 1500 yd

and $x_r = 3500$ yd are to a high degree of approximation simply

$$0.0621 = P(D \mid 1500, 2000) = \frac{1}{x_{\max} y_{\max}} \int_0^{x_{\max}} \int_0^{y_{\max}} P_1\left(D \mid r = \left[(1500 - x_t)^2 + (2000 - y_t)^2\right]^{1/2}\right) dx_t\, dy_t,$$

$$0.0164 = P(D \mid 3500, 2000) = \frac{1}{x_{\max} y_{\max}} \int_0^{x_{\max}} \int_0^{y_{\max}} P_2\left(D \mid r = \left[(3500 - x_t)^2 + (2000 - y_t)^2\right]^{1/2}\right) dx_t\, dy_t,$$

where $P_1(D \mid r)$ and $P_2(D \mid r)$ are the lateral range curves that govern sonar performance shown in figure 6.15. A logical question to ask at this point is the following: Why are these probabilities of detection so small? The answer is that $P(D \mid x_r, y_r)$ depends on the integrated product of sensor lateral range times target probability density. In this case the target probability density is proportional to the product $1/(x_{\max} y_{\max})$. When the target probability density is spread our over a wide area, $P(D \mid x_r, y_r)$ can be small in spite of favorable sensor lateral range characteristics. If no target is present, then sensor probability of detection is zero.

A much more favorable view of sonar performance can be obtained by making the target probability distribution dependent upon receiver location and assuming that the target is uniformly distributed in range and azimuth out to some maximum range that is pegged to sonar performance. For our mine-hunting sonar, this maximum range would be perhaps $r_{\max} = 1000$ yd. Now the probabilities of detection at the receiver locations (1500 yd, 2000 yd) and (3500 yd, 2000 yd) would be

$$0.394 = \frac{1}{\frac{1}{2} r_{\max}^2} \int_0^{r_{\max}} P_1(D \mid r)\, r\, dr,$$

$$0.104 = \frac{1}{\frac{1}{2} r_{\max}^2} \int_0^{r_{\max}} P_2(D \mid r)\, r\, dr.$$

These latter probabilities are five times larger. Which is correct? The answer to this question depends on the application. If all that is required is a relative measure of sonar performance then the latter approach is fine. However, if you require probabilities that correspond to physically realizable engagement scenarios, then the latter approach is totally inappropriate. In this case the performance surface value $P(D \mid x_r, y_r)$ should be computed via

$$P(D \mid x_r, y_r) = \int_0^{x_{\max}} \int_0^{y_{\max}} P(D \mid x_r, y_r, x_t, y_t)\, P(x_t, y_t)\, dx_t\, dy_t,$$

and the target probability distribution must be independent of the receiver location.

References

Blake, Lamont V. (1991), *Radar Range-Performance Analysis*, Munro Publishing Co.

Brekhovskikh, L. and Lysanov, Yu. (1982), *Fundamentals of Ocean Acoustics*, Springer Verlag.

Burdic, William S. (1984), *Underwater Acoustic System Analysis*, Prentice-Hall.

Elmore, W.C. and Heald, A.H. (1969), *Physics of Waves*, Dover Publications.

Gregory, Phil (2005), *Bayesian Logical Data Analysis for the Physical Sciences,* Cam ridge University Press.

Hammersley, J.M. and Handscomb, D.C. (1964), *Monte Carlo Methods*, Chapman and Hall.

Hogg, R.V. and Tanis, E.A. (2006), *Probability and Statistical Inference*, Pearson Prentice Hall, 7th edition.

Hudson, J.A. (1980), *The Excitation and Propagation of Elastic Waves*, Cambridge University Press.

Jaynes, E.T. (2003), *Probability Theory: The Logic of Science*, edited by G. Larry Bretthorst, Cambridge University Press, reprinted 2009.

Jeffreys, Harold, (1973), *Scientific Inference*, Cambridge University Press, 3rd edition.

Jeffreys, Harold, (1976), *The Earth: Its Origin, History and Physical Constitution*, Cambridge University Press, 6th edition.

Jensen, F.B., Kuperman, W.A., Porter, M.B. and Schmidt, H. (1994), *Computational Ocean Acoustics*, American Institute of Physics.

Kimall, G.E. and Morse, P. M. (1970), *Methods of Operations Research*, Peninsula Publishing.

Koopman, Bernard O. (1980), *Search and Screening*, Pergamon Press, republished by The Military Operations Research Society 1999.

Officer, C.B. (1958), *Introduction to the Theory of Sound Transmission*, McGraw-Hill Book Company.

Ol'shevskii, V.V. (1978), *Statistical Methods in Sonar*, technical editor David Middleton, Studies in Soviet Science, Consultants Bureau.

Rees, W.G. (2001), *Physical Principles of Remote Sensing*, Cambridge University Press, 2nd edition.

Ross, Sheldon M. (1972), *Introduction to Probability Models*, Academic Press.

Selin, Ivan. (1965), *Detection Theory*, Princeton University Press.

Skudrzyk, E. (1971), *The Foundations of Acoustics*, Springer-Verlag.

Tucker, D.G. and Gazey, B.K. (1977), *Applied Underwater Acoustics*, Pergamon Press.

Urick, Robert J. (1983), *Principles of Underwater Sound*, McGraw-Hill Book Company.

Whalen, Anthony D. (1971), *Detection of Signals in Noise*, Academic Press.